

Measurement of the final states $\omega\pi^0$, $\rho\eta$, and $\rho\eta'$ from $\psi(2S)$ electromagnetic decays and e^+e^- annihilations

M. Ablikim¹, J. Z. Bai¹, Y. Ban¹¹, J. G. Bian¹, X. Cai¹, J. F. Chang¹, H. F. Chen¹⁷, H. S. Chen¹, H. X. Chen¹, J. C. Chen¹, Jin Chen¹, Jun Chen⁷, M. L. Chen¹, Y. B. Chen¹, S. P. Chi², Y. P. Chu¹, X. Z. Cui¹, H. L. Dai¹, Y. S. Dai¹⁹, Z. Y. Deng¹, L. Y. Dong^{1a}, Q. F. Dong¹⁵, S. X. Du¹, Z. Z. Du¹, J. Fang¹, S. S. Fang², C. D. Fu¹, H. Y. Fu¹, C. S. Gao¹, Y. N. Gao¹⁵, M. Y. Gong¹, W. X. Gong¹, S. D. Gu¹, Y. N. Guo¹, Y. Q. Guo¹, Z. J. Guo¹⁶, F. A. Harris¹⁶, K. L. He¹, M. He¹², X. He¹, Y. K. Heng¹, H. M. Hu¹, T. Hu¹, G. S. Huang^{1b}, X. P. Huang¹, X. T. Huang¹², X. B. Ji¹, C. H. Jiang¹, X. S. Jiang¹, D. P. Jin¹, S. Jin¹, Y. Jin¹, Yi Jin¹, Y. F. Lai¹, F. Li¹, G. Li², H. H. Li¹, J. Li¹, J. C. Li¹, Q. J. Li¹, R. Y. Li¹, S. M. Li¹, W. D. Li¹, W. G. Li¹, X. L. Li⁸, X. Q. Li¹⁰, Y. L. Li⁴, Y. F. Liang¹⁴, H. B. Liao⁶, C. X. Liu¹, F. Liu⁶, Fang Liu¹⁷, H. H. Liu¹, H. M. Liu¹, J. Liu¹¹, J. B. Liu¹, J. P. Liu¹⁸, R. G. Liu¹, Z. A. Liu¹, Z. X. Liu¹, F. Lu¹, G. R. Lu⁵, H. J. Lu¹⁷, J. G. Lu¹, C. L. Luo⁹, L. X. Luo⁴, X. L. Luo¹, F. C. Ma⁸, H. L. Ma¹, J. M. Ma¹, L. L. Ma¹, Q. M. Ma¹, X. B. Ma⁵, X. Y. Ma¹, Z. P. Mao¹, X. H. Mo¹, J. Nie¹, Z. D. Nie¹, S. L. Olsen¹⁶, H. P. Peng¹⁷, N. D. Qi¹, C. D. Qian¹³, H. Qin⁹, J. F. Qiu¹, Z. Y. Ren¹, G. Rong¹, L. Y. Shan¹, L. Shang¹, D. L. Shen¹, X. Y. Shen¹, H. Y. Sheng¹, F. Shi¹, X. Shi^{11c}, H. S. Sun¹, J. F. Sun¹, S. S. Sun¹, Y. Z. Sun¹, Z. J. Sun¹, X. Tang¹, N. Tao¹⁷, Y. R. Tian¹⁵, G. L. Tong¹, G. S. Varner¹⁶, D. Y. Wang¹, J. Z. Wang¹, K. Wang¹⁷, L. Wang¹, L. S. Wang¹, M. Wang¹, P. Wang¹, P. L. Wang¹, S. Z. Wang¹, W. F. Wang^{1d}, Y. F. Wang¹, Z. Wang¹, Z. Y. Wang¹, Zhe Wang¹, Zheng Wang², C. L. Wei¹, D. H. Wei¹, N. Wu¹, Y. M. Wu¹, X. M. Xia¹, X. X. Xie¹, B. Xin^{8b}, G. F. Xu¹, H. Xu¹, S. T. Xue¹, M. L. Yan¹⁷, F. Yang¹⁰, H. X. Yang¹, J. Yang¹⁷, Y. X. Yang³, M. Ye¹, M. H. Ye², Y. X. Ye¹⁷, L. H. Yi⁷, Z. Y. Yi¹, C. S. Yu¹, G. W. Yu¹, C. Z. Yuan¹, J. M. Yuan¹, Y. Yuan¹, S. L. Zang¹, Y. Zeng⁷, Yu Zeng¹, B. X. Zhang¹, B. Y. Zhang¹, C. C. Zhang¹, D. H. Zhang¹, H. Y. Zhang¹, J. Zhang¹, J. W. Zhang¹, J. Y. Zhang¹, Q. J. Zhang¹, S. Q. Zhang¹, X. M. Zhang¹, X. Y. Zhang¹², Y. Y. Zhang¹, Yiyun Zhang¹⁴, Z. P. Zhang¹⁷, Z. Q. Zhang⁵, D. X. Zhao¹, J. B. Zhao¹, J. W. Zhao¹, M. G. Zhao¹⁰, P. P. Zhao¹, W. R. Zhao¹, X. J. Zhao¹, Y. B. Zhao¹, Z. G. Zhao^{1e}, H. Q. Zheng¹¹, J. P. Zheng¹, L. S. Zheng¹, Z. P. Zheng¹, X. C. Zhong¹, B. Q. Zhou¹, G. M. Zhou¹, L. Zhou¹, N. F. Zhou¹, K. J. Zhu¹, Q. M. Zhu¹, Y. C. Zhu¹, Y. S. Zhu¹, Yingchun Zhu^{1f}, Z. A. Zhu¹, B. A. Zhuang¹, X. A. Zhuang¹, B. S. Zou¹.

(BES Collaboration)

¹ Institute of High Energy Physics, Beijing 100049, People's Republic of China

² China Center for Advanced Science and Technology(CCAST), Beijing 100080, People's Republic of China

³ Guangxi Normal University, Guilin 541004, People's Republic of China

⁴ Guangxi University, Nanning 530004, People's Republic of China

⁵ Henan Normal University, Xinxiang 453002, People's Republic of China

⁶ Huazhong Normal University, Wuhan 430079, People's Republic of China

⁷ Hunan University, Changsha 410082, People's Republic of China

⁸ Liaoning University, Shenyang 110036, People's Republic of China

⁹ Nanjing Normal University, Nanjing 210097, People's Republic of China

¹⁰ Nankai University, Tianjin 300071, People's Republic of China

¹¹ Peking University, Beijing 100871, People's Republic of China

¹² Shandong University, Jinan 250100, People's Republic of China

¹³ Shanghai Jiaotong University, Shanghai 200030, People's Republic of China

¹⁴ Sichuan University, Chengdu 610064, People's Republic of China

¹⁵ Tsinghua University, Beijing 100084, People's Republic of China

¹⁶ University of Hawaii, Honolulu, HI 96822, USA

¹⁷ University of Science and Technology of China, Hefei 230026, People's Republic of China

¹⁸ Wuhan University, Wuhan 430072, People's Republic of China

¹⁹ Zhejiang University, Hangzhou 310028, People's Republic of China

^a Current address: Iowa State University, Ames, IA 50011-3160, USA.

^b Current address: Purdue University, West Lafayette, IN 47907, USA.

^c Current address: Cornell University, Ithaca, NY 14853, USA.

^d Current address: Laboratoire de l'Accélérateur Linéaire, F-91898 Orsay, France.

^e Current address: University of Michigan, Ann Arbor, MI 48109, USA.

^f Current address: DESY, D-22607, Hamburg, Germany.

Cross sections and form factors for $e^+e^- \rightarrow \omega\pi^0$, $\rho\eta$, and $\rho\eta'$ at center of mass energies of 3.650, 3.686, and 3.773 GeV are measured using data samples collected with the BESII detector at the BEPC. Also, the branching fractions of $\psi(2S) \rightarrow \omega\pi^0$, $\rho\eta$, and $\rho\eta'$ are determined to be $(1.87_{-0.62}^{+0.68} \pm 0.28) \times 10^{-5}$, $(1.78_{-0.62}^{+0.67} \pm 0.17) \times 10^{-5}$, and $(1.87_{-1.11}^{+1.64} \pm 0.33) \times 10^{-5}$, respectively.

PACS numbers: 13.25.Gv, 12.38.Qk, 13.40.Gp

I. INTRODUCTION

Form factors of the electromagnetic processes $\psi(2S) \rightarrow \omega\pi^0$ ($\rho\eta$, $\rho\eta'$) provide information on the strength of the electromagnetic amplitude in $\psi(2S) \rightarrow 1^-0^-$ decays. Such information is indispensable to separate the strong interaction amplitude for other $\psi(2S) \rightarrow 1^-0^-$ decay modes, and even more importantly, to determine the relative phase between the electromagnetic and strong amplitudes [1]. This phase has been found to be orthogonal in virtually all J/ψ decays, such as 1^+0^- [2], 1^-0^- [3, 4], 0^-0^- [5, 6], 1^-1^- [6], and $N\bar{N}$ [7] modes. It is suggested that this orthogonality also exists in $\psi(2S)$ decays and is universal [8].

The Born-order cross section for the electromagnetic process $e^+e^- \rightarrow V + P$ ($\omega\pi^0$, $\rho\eta$, $\rho\eta'$) in continuum production can be expressed as [9]

$$\sigma_{Born}(s) = \frac{4\pi\alpha^2}{s^{3/2}} \cdot |\mathcal{F}_{VP}(s)|^2 \cdot \mathcal{P}_{VP}(s), \quad (1)$$

where $\mathcal{P}_{VP}(s) = \frac{1}{3}q_{VP}^3$, q_{VP} is the momentum of either the Vector or Pseudoscalar meson in the VP decay, and the form factor $|\mathcal{F}_{VP}(s)|$ is an s dependent variable [10, 11].

By measuring the cross section of $e^+e^- \rightarrow VP$ in continuum production and correcting for the effect of initial state radiation, the form factor $\mathcal{F}_{VP}(s)$ can be determined. In contrast, for $e^+e^- \rightarrow VP$ at the $\psi(2S)$ peak, the total cross section includes contributions from both resonance production and decay and the continuum process, although the interference between them can be neglected [9]. By separating the one-photon annihilation and $\psi(2S)$ resonance contributions, both the form factor at resonance and the branching fractions of $\psi(2S) \rightarrow VP$ can be obtained. The branching fractions of $\psi(2S) \rightarrow \rho\eta$ and $\rho\eta'$ provide useful information on the quark content of η and η' mesons [6].

In this paper, we report measurements for the cross sections and form factors of $\omega\pi^0$, $\rho\eta$, and $\rho\eta'$ at center of mass energies 3.650, 3.686, and 3.773 GeV, and the branching fractions of $\psi(2S) \rightarrow \omega\pi^0$, $\rho\eta$, and $\rho\eta'$ at 3.686 GeV.

II. THE BESII DETECTOR

The Beijing Spectrometer (BESII) is a conventional cylindrical magnetic detector that is described in detail in Ref. [12]. A 12-layer Vertex Chamber (VC) surrounding the beryllium beam pipe provides input to the event trigger, as well as coordinate information. A forty-layer main drift chamber (MDC) located just outside the VC yields precise measurements of charged particle trajectories with a solid angle coverage of 85% of 4π ; it also provides ionization energy loss (dE/dx) measurements which are used for particle identification. Momentum resolution of $1.7\%\sqrt{1+p^2}$ (p in GeV/ c) and dE/dx resolution for hadron tracks of $\sim 8\%$ are obtained. An array of 48 scintillation counters surrounding the MDC measures the time of flight (TOF) of charged particles with a resolution of about 200 ps for hadrons. Outside the TOF counters, a 12 radiation length, lead-gas barrel shower counter (BSC), operating in limited streamer mode, measures the energies of electrons and photons over 80% of the total solid angle with an energy resolution of $\sigma_E/E = 0.22/\sqrt{E}$ (E in GeV). A solenoidal magnet outside the BSC provides a 0.4 T magnetic field in the central tracking region of the detector. Three double-layer muon counters instrument the magnet flux return and serve to identify muons with momentum greater than 500 MeV/ c . They cover 68% of the total solid angle.

In this analysis, a GEANT3 based Monte Carlo package (SIMBES) with detailed consideration of the detector performance (such as dead electronic chan-

nels) is used. The consistency between data and Monte Carlo (MC) has been carefully checked in many high purity physics channels, and the agreement is reasonable. The generators **EE2VP** [13] and **HOWL-VP** [14], together with SIMBES, are used to determine the detection efficiencies for the one photon annihilation and resonance decay processes.

III. EVENT SELECTION

The data samples used for this analysis consist of 14.0×10^6 ($1 \pm 4\%$) $\psi(2S)$ events [15], 6.42 ($1 \pm 4\%$) pb^{-1} of continuum data at $\sqrt{s} = 3.650$ GeV [16], and 17.3 ($1 \pm 3\%$) pb^{-1} at the $\psi(3770)$ [17]. The channels studied are $\omega\pi^0$, $\rho\eta$, and $\rho\eta'$, where ω decays to $\pi^+\pi^-\pi^0$, ρ to $\pi^+\pi^-$, η to $\gamma\gamma$, and η' to $\eta\pi^+\pi^-$.

A neutral cluster is considered to be a photon candidate if it is located within the BSC fiducial region, the energy deposited in the BSC is greater than 50 MeV, the first hit appears in the first 6 radiation lengths, and the angle between the cluster development direction in the BSC and the photon emission direction from the beam interaction point (IP) is less than 37° . For the $\rho\eta$ channel, tighter requirements are applied: the energy deposited in the BSC must be greater than 100 MeV, and the angle in the xy plane (perpendicular to beam direction) between the neutral cluster and the nearest charged track must be greater than 15° .

Each charged track is required to be well fit by a three-dimensional helix, to originate from the IP region, $V_{xy} = \sqrt{V_x^2 + V_y^2} < 2$ cm and $|V_z| < 20$ cm, and to have a polar angle $|\cos\theta| < 0.8$. Here V_x , V_y , and V_z are the x, y, and z coordinates of the point of the closest approach of the track to the beam axis.

The TOF and dE/dx measurements for each charged track are used to calculate $\chi_{PID}^2(i)$ values and the corresponding confidence levels $Prob_{PID}(i)$ for the hypotheses that a track is a pion, kaon, or proton, where i ($i = \pi/K/p$) is the particle type. For events involving the final state $\omega\pi^0$ and $\rho\eta'$, at least half of charged pion candidates in each event are required to have $Prob_{PID}(\pi)$ larger than 0.01, while for events involving the final state $\rho\eta$, both charged pion candidates must satisfy this requirement.

A. $\omega\pi^0$ channel

For this channel, the events are required to have two good charged tracks with net charge zero and four or five photon candidates. A four constraint (4C) kinematic fit under the hypothesis $e^+e^- \rightarrow \pi^+\pi^-\gamma\gamma\gamma\gamma$ is

performed. If the number of selected photons is larger than four, the fit is repeated using all possible combinations of photons, and the one with the smallest χ^2 is chosen. The confidence level of the 4C fit is required to be larger than 0.01. In addition, we require that χ_{com}^2 [18] for the assignment $e^+e^- \rightarrow \pi^+\pi^-\gamma\gamma\gamma\gamma$ must be smaller than that for $e^+e^- \rightarrow K^+K^-\gamma\gamma\gamma\gamma$ in order to suppress possible $K^+K^-4\gamma$ background.

Among the four selected photons, there are three possible combinations to compose two π^0 s: $(\gamma_1\gamma_2, \gamma_3\gamma_4)$, $(\gamma_1\gamma_3, \gamma_2\gamma_4)$, and $(\gamma_1\gamma_4, \gamma_2\gamma_3)$. Events where one and only one combination have both π^0 candidates satisfying $|M_{\gamma\gamma} - 0.135| < 0.05$ GeV/ c^2 are kept for further analysis.

Using the above selection, $\pi^+\pi^-\pi^0\pi^0$ candidate events are obtained. Fig. 1 shows the $\pi^+\pi^-\pi_L^0$ invariant mass distributions, where π_L^0 is the lower energy π^0 from the two π^0 candidates. Clear ω signals are seen in all three data samples at $\sqrt{s} = 3.650$, 3.686, and 3.773 GeV.

The $\pi^+\pi^-\pi_L^0$ invariant mass distribution is fit with a shape for the signal determined by MC simulation plus a polynomial background, and $7.3_{-2.7}^{+3.3}$, $31.2_{-6.9}^{+7.7}$, and $8.6_{-3.3}^{+4.0}$ events are observed in the data samples at $\sqrt{s} = 3.650$, 3.686, and 3.773 GeV, with 3.9σ , 5.6σ , and 3.2σ statistical significance [19], respectively.

B. $\rho\eta$ channel

For this channel, the events are required to have two good charged tracks with net charge zero and two photon candidates. A 4C kinematic fit to the hypothesis $e^+e^- \rightarrow \pi^+\pi^-\gamma\gamma$ is performed, and its confidence level is required to be larger than 0.01 and larger than that for the assignment $K^+K^-\gamma\gamma$ to suppress possible $K^+K^-\gamma\gamma$ background. The energy of each photon is required to be less than 1.7 GeV to reject backgrounds from $\psi(2S) \rightarrow \gamma\eta'$. An additional requirement $|m_{\pi^+\pi^-} - 0.776| < 0.15$ GeV/ c^2 is applied to further suppress background from non- ρ decay. Fig. 2 shows the $\gamma\gamma$ invariant mass distributions for $\rho\gamma\gamma$ candidate events. Clear η signals are seen in all three data samples at $\sqrt{s} = 3.650$, 3.686, and 3.773 GeV.

The $m_{\gamma\gamma}$ invariant mass spectrum is fitted with a shape for the η signal determined by MC simulation plus a polynomial background, and $2.3_{-1.4}^{+2.1}$, $29.2_{-6.8}^{+7.5}$, and $5.8_{-2.6}^{+3.3}$ events are observed in the data samples at $\sqrt{s} = 3.650$, 3.686, and 3.773 GeV, respectively. The statistical significances are 1.9σ , 5.5σ , and 3.3σ , respectively.

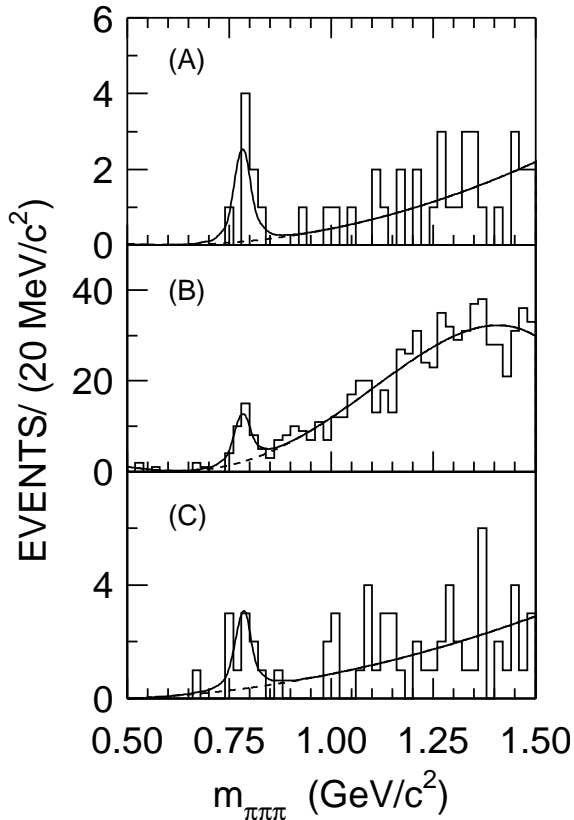


FIG. 1: The $\pi^+\pi^-\pi_L^0$ invariant mass distributions for $e^+e^- \rightarrow \pi^+\pi^-\pi_L^0\pi_H^0$ candidate events at $\sqrt{s} =$ (A) 3.650, (B) 3.686, and (C) 3.773 GeV. π_L^0 and π_H^0 are the low and high energy pions. The curves show the fit described in the text.

C. $\rho\eta'$ channel

Here, events with four good charged tracks with net charge zero and two or three photon candidates are selected. A 4C kinematic fit is performed for the hypothesis $\pi^+\pi^-\pi^+\pi^-\gamma\gamma$. If the number of selected photons is larger than 2, the fit is repeated using all combinations of photons, and the one with the smallest χ^2 is chosen. The confidence level of the 4C fit is required to be larger than 0.01 and larger than that for $K^+K^-\pi^+\pi^-\gamma\gamma$. The two photons are required to come from η decay ($|m_{\gamma\gamma} - 0.548| < 0.05$ GeV/ c^2). Background from $\psi(2S) \rightarrow \pi^+\pi^-J/\psi$ is rejected with the requirement that the mass recoiling from any $\pi^+\pi^-$ pair satisfies $|m_{recoil}^{\pi^+\pi^-} - 3.1| > 0.05$ GeV/ c^2 . In order to suppress background from non- ρ decay, an additional requirement $|m_{\pi^+\pi^-} - 0.776| < 0.15$ GeV/ c^2 is applied, where $m_{\pi^+\pi^-}$ runs over all possible $\pi^+\pi^-$ pairs. Fig. 3 shows the $\eta\pi^+\pi^-$ invariant mass distributions for $\rho\pi^+\pi^-\eta$ candidate events. $5.4_{-2.2}^{+3.3}$ events are obtained in the data sample at

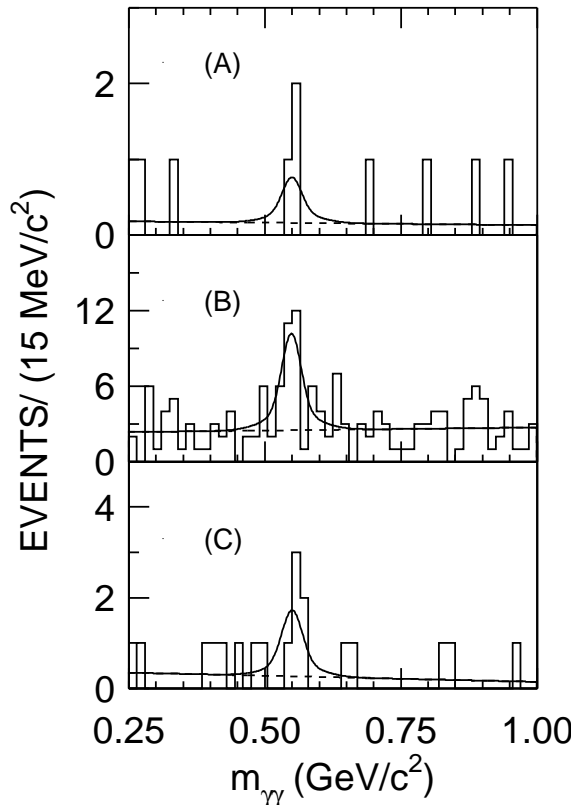


FIG. 2: The $\gamma\gamma$ invariant mass distributions for $e^+e^- \rightarrow \rho\gamma\gamma$ candidate events at $\sqrt{s} =$ (A) 3.650, (B) 3.686, and (C) 3.773 GeV. The curves show the fit described in the text.

$\sqrt{s} = 3.686$ GeV by fitting the $\eta\pi^+\pi^-$ invariant mass spectrum with an η' shape obtained by MC simulation plus a polynomial for background. The statistical significance for the η' signal is 3.1σ . Only 1 event is observed in each of the two data samples at $\sqrt{s} = 3.650$ and 3.773 GeV, and the respective background is zero and 0.64 events as estimated from sidebands; the corresponding upper limit for the observed $\rho\eta'$ event is calculated to be 4.4 and 3.9 events, respectively, with the scheme of J. Conrad *et al.* [20].

IV. SEPARATION OF CONTINUUM AND RESONANCE EVENTS

At the $\psi(2S)$ peak, the cross section is from resonance decay, one-photon annihilation, and their interference, all electromagnetic processes. The observed events are separated for the $\psi(2S)$ decay and one-photon annihilation processes using the scheme proposed by P. Wang *et al.* [9], considering the detection-efficiency difference between the resonance decay and

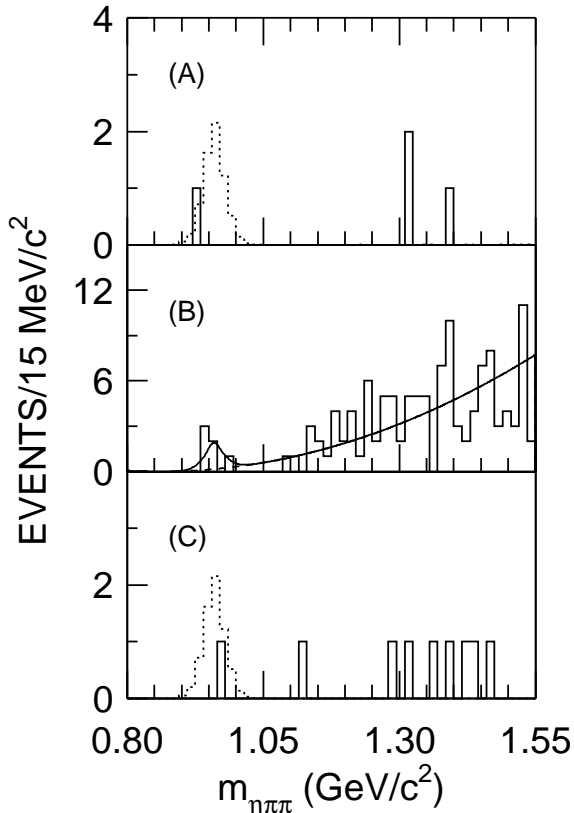


FIG. 3: The $\eta\pi^+\pi^-$ invariant mass distributions for $e^+e^- \rightarrow \rho\pi^+\pi^-\eta$ candidate events (solid histogram) and $e^+e^- \rightarrow \rho\eta'$ Monte Carlo simulation (dotted histogram) with arbitrary normalization for $\sqrt{s} =$ (A) 3.650, (B) 3.686, and (C) 3.773 GeV. The curve in (B) shows the fit described in the text.

one-photon annihilation, and neglecting the tiny interference (see Table I), that is,

$$N^{obs} = \mathcal{L} \cdot (\sigma^{\psi(2S)} \cdot \epsilon^{\psi(2S)} + \sigma^{Cont.} \cdot \epsilon^{Cont.}),$$

where \mathcal{L} is the integrated luminosity, σ the cross section, and ϵ the detection efficiency. Table I lists detailed information on the separation of the signal events observed in the data sample at $\sqrt{s} = 3.686$ GeV.

For the data sample at $\sqrt{s} = 3.650$ GeV, the fraction of cross section from the $\psi(2S)$ resonance is negligible ($< 1.1 \times 10^{-4}$) compared to that of the continuum, as estimated using the scheme proposed by P. Wang *et al.* [9]. Therefore we attribute all observed events to one-photon annihilation.

For the data sample at $\sqrt{s} = 3.773$ GeV, the resonance part of the cross section for $e^+e^- \rightarrow \psi(3770) \rightarrow VP$ ($\omega\pi^0$, $\rho\eta$, $\rho\eta'$), at Born order, is

$$\sigma_{Born}(s) = \frac{12\pi\Gamma_{ee}\Gamma_f}{(s - M^2)^2 + \Gamma_t^2 M^2}, \quad (2)$$

where Γ_f is the partial width to the final state f ($\omega\pi^0$, $\rho\eta$, $\rho\eta'$) and is related to Γ_{ee} and the corresponding form factor is [9]:

$$\Gamma_f = \frac{\Gamma_{ee}q_f^3}{m_{\psi(3770)}} |\mathcal{F}_f(m_{\psi(3770)}^2)|^2.$$

Since Γ_t and Γ_{ee} of $\psi(3770)$ are 23.6 ± 2.7 MeV/ c^2 and 0.26 ± 0.04 keV/ c^2 , respectively [21], the fraction of the cross section from $\psi(3770)$ resonance production is negligible ($\approx 2.1 \times 10^{-5}$) compared to that from one-photon annihilation. The $\psi(2S)$ tail at $\sqrt{s} = 3.773$ GeV contributes no more than 2.0% for the observed events in these final states. Therefore, the observed events are taken to be totally from one-photon annihilation.

V. SYSTEMATIC ERROR

Many sources of systematic error are considered. Systematic errors associated with the efficiency are determined by comparing J/ψ and $\psi(2S)$ data with Monte Carlo simulations for very clean decay channels, such as $J/\psi \rightarrow \rho\pi$, $\omega\pi^0$ and $\psi(2S) \rightarrow \pi^+\pi^-J/\psi$, which allows the determination of systematic errors associated with the MDC tracking efficiency, kinematic fitting and photon selection efficiencies, etc. [22]

To investigate possible background channels, we utilize three Monte Carlo samples : I) continuum channels from u , d , and s quark fragmentation generated with JETSET7.4 [23]; II) $\psi(2S) \rightarrow anything$ generated with LUND-charm generator [24]; and III) $D\bar{D}$ pairs generated at $\sqrt{s} = 3.773$ GeV. From these MC samples, we find that the background contaminations are negligible in the three data samples, except for the $\omega\pi^0$ channel at $\sqrt{s} = 3.686$ GeV. Events from $\psi(2S) \rightarrow b_1^0\pi^0$ and cascade decays $\psi(2S) \rightarrow anything+J/\psi$, $J/\psi \rightarrow \rho^0\pi^0$ can produce background in the M_ω mass region. The resulting estimate of contamination from these sources is $N_{bkg} = 1.6 \pm 0.7$, and the corresponding systematic error is $(5.1 \pm 2.3)\%$. We take 7% as a conservative estimation and treat it as one source of systematic error for the $\omega\pi^0$ channel at $\sqrt{s} = 3.686$ GeV.

Different s dependences of the form factor ($\frac{1}{s}$ versus $\frac{1}{s^2}$) result in changes of 2.5%, which is taken as one of the systematic errors. The uncertainties of the generators, background shapes, and luminosities are also included. Table II lists all the sources of systematic errors, and the total systematic error is taken as the sum of the individual terms added in quadrature.

TABLE I: Cross section and event fractions for the $\psi(2S)$ production and decay and one-photon annihilation processes for $\omega\pi^0$, $\rho\eta$, and $\rho\eta'$ final states at $\sqrt{s} = 3.686$ GeV. ϵ is the detection efficiency determined from MC simulation.

	$\omega\pi^0$		$\rho\eta$		$\rho\eta'$		Int.
	$\psi(2S)$	Cont.	$\psi(2S)$	Cont.	$\psi(2S)$	Cont.	
σ frac. (%)	40.6	60.7	40.6	60.7	40.8	60.5	-1.3
ϵ (%)	5.97	4.98	13.43	10.89	5.48	4.43	-
N^{obs} frac. (%)	44.5	55.5	45.2	54.8	45.5	54.5	-
N^{obs}	$13.9^{+5.1}_{-4.6}$	$17.3^{+5.7}_{-5.1}$	$13.2^{+5.0}_{-4.6}$	$16.0^{+5.6}_{-5.0}$	$2.5^{+2.2}_{-1.5}$	$2.9^{+2.4}_{-1.6}$	-

TABLE II: Summary of systematic errors (%). D1, D2, and D3 represent the data samples at $\sqrt{s} = 3.65$, 3.686, and 3.773 GeV, respectively.

Sample	$\omega\pi^0$			$\rho\eta$			$\rho\eta'$		
	D1	D2	D3	D1	D2	D3	D1	D2	D3
Tracking	4.0	4.0	4.0	4.0	4.0	4.0	8.0	8.0	8.0
Photon	8.0	8.0	8.0	4.0	4.0	4.0	4.0	4.0	4.0
Kine. fit.	4.0	4.0	4.0	4.0	4.0	4.0	4.0	4.0	4.0
Bg. contam.	0.0	7.0	0.0	0.0	0.0	0.0	0.0	0.0	0.0
Bg. shape	13.6	7.3	11.6	9.6	4.5	6.3	0.0	13.3	0.0
Luminosity	4.0	4.0	3.0	4.0	4.0	3.0	4.0	4.0	3.0
$B(X \rightarrow Y)$	0.8	0.8	0.8	0.7	0.7	0.7	3.4	3.4	3.4
MC fluct.	1.4	1.4	1.4	1.3	1.3	1.3	2.1	2.1	2.1
Generator	1.3	1.3	1.3	3.4	3.4	3.4	2.8	2.8	2.8
$\mathcal{F}_{VP}(s)$	2.5	2.5	2.5	2.5	2.5	2.5	2.5	2.5	2.5
Sum (σ^{sys})	17.5	15.0	15.8	13.3	10.2	10.8	11.9	17.9	11.6

VI. RESULTS AND DISCUSSION

The Born order cross sections for $e^+e^- \rightarrow X$ are calculated from

$$\sigma_{Born} = \frac{N_{e^+e^- \rightarrow X \rightarrow Y}^{obs}}{B(X \rightarrow Y)\mathcal{L} \cdot \epsilon^{MC} \cdot (1 + \delta)}, \quad (3)$$

where $N_{e^+e^- \rightarrow X \rightarrow Y}^{obs}$ is the number of observed events in the final state from one photon annihilation, X is the intermediate state, Y is the final state, ϵ is the detection efficiency obtained from the MC simulation, \mathcal{L} is the integrated luminosity, and δ is the radiative correction calculated according to Ref. [25]. With the cross section of $e^+e^- \rightarrow VP$ ($\omega\pi^0$, $\rho\eta$, $\rho\eta'$) from Eq. (3) and using Eq. (1), we obtain $|\mathcal{F}_{VP}|$ at $\sqrt{s} = 3.650$, 3.686, and 3.773 GeV.

The branching fraction for $\psi(2S) \rightarrow X$ is calculated from

$$B(\psi(2S) \rightarrow X) = \frac{N_{\psi(2S) \rightarrow X \rightarrow Y}^{obs}}{N_{\psi(2S)} \cdot B(X \rightarrow Y) \cdot \epsilon^{MC}}, \quad (4)$$

where $N_{\psi(2S) \rightarrow X \rightarrow Y}^{obs}$ is the number of observed events in the final state from $\psi(2S)$ decay.

Tables III and IV summarize the results for $e^+e^- \rightarrow \omega\pi^0$, $\rho\eta$, and $\rho\eta'$ at $\sqrt{s} = 3.650$, 3.686, and 3.773 GeV,

and the branching fractions of $\psi(2S) \rightarrow \omega\pi^0$, $\rho\eta$, and $\rho\eta'$ at 3.686 GeV. The ratios of $\psi(2S)$ to J/ψ branching fractions are also listed in Table IV, where the J/ψ branching fractions are taken from the PDG [21].

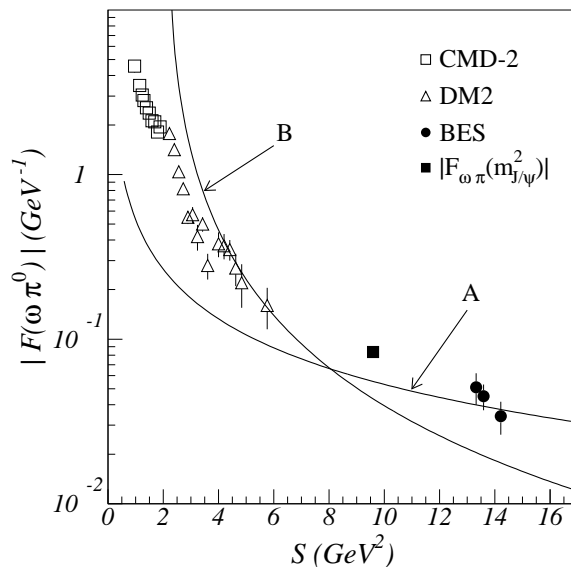


FIG. 4: Energy dependence of the $e^+e^- \rightarrow \gamma^* \rightarrow \omega\pi^0$ form factor. Curve (A) is calculated with Eq. (6), while curve (B) is calculated with Eq. (7).

Fig. 4 shows the measured results of $|\mathcal{F}_{\omega\pi^0}|$ from our measurements, CMD-2 [26], and DM2 [27], and the calculated value of $|\mathcal{F}_{\omega\pi^0}|$ at $s = m_{J/\psi}^2$ [4]:

$$\frac{|\mathcal{F}_{\omega\pi^0}(m_{J/\psi}^2)|^2}{|\mathcal{F}_{\omega\pi^0}(0)|^2} = \frac{\frac{\alpha}{3} \left(\frac{p_\pi}{p_\omega}\right)^3 \cdot m_{J/\psi} \cdot \Gamma(\psi(2S) \rightarrow \omega\pi^0)}{\Gamma(\omega \rightarrow \gamma\pi^0) \cdot \Gamma(J/\psi \rightarrow \mu^+\mu^-)}, \quad (5)$$

where $|\mathcal{F}_{\omega\pi^0}(0)| = 2.3$ GeV $^{-1}$ [10], and the other quantities are taken from the PDG [21]. Curve (A) is predicted by J.-M. Gérard and G. López Castro [11] as:

$$|\mathcal{F}_{\omega\pi^0}(s \rightarrow \infty)| = \frac{f_\omega f_\pi}{3\sqrt{2}s}, \quad (6)$$

with the decay constants of ω and π of $f_\omega = 17.05 \pm 0.28$ and $f_\pi = 0.1307$ GeV. Curve (B) is predicted by

TABLE III: Cross sections and form factors measured for $e^+e^- \rightarrow \omega\pi^0$, $\rho\eta$, and $\rho\eta'$ at $\sqrt{s} = 3.650, 3.686$, and 3.773 GeV.

Channel	Samples	\mathcal{L} (pb $^{-1}$)	$N_{Cont.}^{obs}$	ϵ (%)	$1 + \delta$	σ_0 (pb)	$ \mathcal{F}_{VP} $ (GeV $^{-1}$)
$\omega\pi^0$	3.650 GeV	6.42	$7.3^{+3.3}_{-2.7}$	5.09	1.032	$24.3^{+11.0}_{-9.0} \pm 4.3$	$0.051^{+0.12}_{-0.10}$
	3.686 GeV	19.72	$17.3^{+5.7}_{-5.1}$	4.98	1.031	$19.2^{+6.3}_{-5.7} \pm 2.9$	$0.045^{+0.008}_{-0.007}$
	3.773 GeV	17.3	$8.6^{+4.0}_{-3.3}$	5.09	1.028	$10.7^{+5.0}_{-4.1} \pm 1.7$	$0.034^{+0.008}_{-0.007}$
$\rho\eta$	3.650 GeV	6.42	$2.3^{+2.1}_{-1.4}$	10.9	1.028	$8.1^{+7.4}_{-4.9} \pm 1.1$	$0.030^{+0.014}_{-0.009}$
	3.686 GeV	19.72	$16.0^{+5.6}_{-5.0}$	10.9	1.028	$18.4^{+8.6}_{-7.8} \pm 1.9$	$0.046^{+0.011}_{-0.010}$
	3.773 GeV	17.3	$5.8^{+3.3}_{-2.6}$	10.7	1.026	$7.8^{+4.4}_{-3.5} \pm 0.08$	$0.030^{+0.009}_{-0.007}$
$\rho\eta'$	3.650 GeV	6.42	< 4.4	4.33	1.021	< 89	< 0.192
	3.686 GeV	19.72	$2.9^{+2.4}_{-1.6}$	4.43	1.020	$18.6^{+15.4}_{-10.3} \pm 3.6$	$0.050^{+0.021}_{-0.015}$
	3.773 GeV	17.3	< 3.9	4.56	1.019	< 28	< 0.106

TABLE IV: Branching fractions measured for $\psi(2S) \rightarrow \omega\pi^0$, $\rho\eta$, and $\rho\eta'$. The corresponding J/ψ branching fractions [21] and the ratios $Q_h = \frac{B(\psi(2S) \rightarrow h)}{B(J/\psi \rightarrow h)}$ are also given.

Channel	$N_{\psi(2S)}$	$N_{Res.}^{obs}$	ϵ (%)	$\mathcal{B}_{\psi(2S) \rightarrow h} (\times 10^{-5})$	$\mathcal{B}_{J/\psi \rightarrow h} (\times 10^{-4})$	Q_h (%)
$\omega\pi^0$	1.4×10^7	$13.9^{+5.1}_{-4.6}$	5.97	$1.87^{+0.68}_{-0.62} \pm 0.28$	4.2 ± 0.6	$4.4^{+1.8}_{-1.6}$
$\rho\eta$	1.4×10^7	$13.2^{+5.0}_{-4.6}$	13.43	$1.78^{+0.67}_{-0.62} \pm 0.17$	1.93 ± 0.23	$9.2^{+3.6}_{-3.3}$
$\rho\eta'$	1.4×10^7	$2.5^{+2.2}_{-1.5}$	5.48	$1.87^{+1.64}_{-1.11} \pm 0.33$	1.05 ± 0.18	$17.8^{+15.9}_{-11.1}$

Victor Chernyak [10]:

$$|\mathcal{F}_{\omega\pi^0}(s)| = |\mathcal{F}_{\omega\pi^0}(0)| \frac{m_\rho^2 M_{\rho'}^2}{(m_\rho^2 - s)(M_{\rho'}^2 - s)}, \quad (7)$$

where m_ρ and $M_{\rho'}$ are the masses of $\rho(770)$ and $\rho(1450)$, respectively. From Fig. 4, our results agree with the description of Eq. (6).

VII. SUMMARY

In conclusion, we determine branching fractions for $\psi(2S) \rightarrow \omega\pi^0$, $\rho\eta$, and $\rho\eta'$ and the form factors $\mathcal{F}_{\omega\pi^0}$, $\mathcal{F}_{\rho\eta}$, and $\mathcal{F}_{\rho\eta'}$ at $\sqrt{s} = 3.650, 3.686$, and 3.773 GeV for the first time. The branching fractions of $\psi(2S) \rightarrow \omega\pi^0$ and $\rho\eta$ in our measurement are consistent with those of CLEOc [28].

Acknowledgments

The BES collaboration thanks the staff of BEPC for their hard efforts. This work is supported in part by the National Natural Science Foundation of China under contracts Nos. 19991480, 10225524, 10225525, the Chinese Academy of Sciences under contract No. KJ 95T-03, the 100 Talents Program of CAS under Contract Nos. U-11, U-24, U-25, and the Knowledge Innovation Project of CAS under Contract Nos. U-602, U-34 (IHEP); by the National Natural Science Foundation of China under Contract No. 10175060 (USTC), and No. 10225522 (Tsinghua University); and by the Department of Energy under Contract No. DE-FG03-94ER40833 (U Hawaii).

- | | |
|--|---|
| <p>[1] P. Wang, C. Z. Yuan and X. H. Mo, Phys. Rev. D 69, 057502 (2004).</p> <p>[2] M. Suzuki, Phys. Rev. D 63, 054021 (2001).</p> <p>[3] DM2 Collab., J. Jousset <i>et al.</i>, Phys. Rev. D 41, 1389 (1990).</p> <p>[4] MARK III Collab., D. Coffman <i>et al.</i>, Phys. Rev. D 38, 2695 (1988).</p> <p>[5] M. Suzuki, Phys. Rev. D 60, 051501 (1999).</p> <p>[6] L. Köpke and N. Wermes, Phys. Rep. 174, 67 (1989).</p> <p>[7] FENICE Collab., R. Baldini <i>et al.</i>, Phys. Lett. B 444, 111 (1998).</p> | <p>[8] P. Wang, C. Z. Yuan and X. H. Mo, Phys. Lett. B 574, 41 (2004).</p> <p>[9] P. Wang, X. H. Mo and C. Z. Yuan, Phys. Lett. B 557, 192 (2003).</p> <p>[10] Victor Chernyak, hep-ph/9906387.</p> <p>[11] J.-M. Gérard and G. López Castro, Phys. Lett. B 425, 365 (1998).</p> <p>[12] BES Collab., J. Z. Bai <i>et al.</i>, Nucl. Instr. Meth. A 458, 627 (2001).</p> <p>[13] L. L. Ma <i>et al.</i>, HEP&NP 28, 1021 (2004).</p> <p>[14] In the generator for $\psi(2S)$ decays into VP mesons, the</p> |
|--|---|

angular distribution is described by $\frac{d^3\sigma}{d\cos\theta_V d\cos\theta_1 d\phi_1} = \sin^2\theta_1[1 + \cos^2\theta_V + \sin^2\theta_V \cos(2\phi_1)]$, where θ_V is the angle between the vector meson and the positron direction. For two-body decays, such as $\rho \rightarrow \pi^+\pi^-$, θ_1 and ϕ_1 are the polar and azimuthal angles of the momentum of the π^+ with respect to the helicity direction of the ρ . For $\omega \rightarrow \pi^+\pi^-\pi^0$, θ_1 and ϕ_1 represent the angles of the normal to the decay plane with respect to the helicity direction of the ω .

- [15] X. H. Mo *et al.*, HEP&NP **28**, 455 (2004).
- [16] S. P. Chi, X. H. Mo and Y. S. Zhu, Measurement of the Integrated Luminosity at $\sqrt{s} = 3.650, 3686$ GeV for the BES Detector (to be published at HEP&NP 28 (2004)).
- [17] BES Collab., J. Z. Bai *et al.*, Measurement of cross sections for $D^0\bar{D}^0$ and D^+D^- production in e^+e^- annihilation at $\sqrt{s} = 3.773$ GeV (submitted to Phys. Lett. **B**).
- [18] The combined χ^2 , χ_{com}^2 , is defined as the sum of the χ^2 values of the kinematic fit (χ_{kine}^2) and those from each of all particle identification assignments: $\chi_{com}^2 = \sum_i \chi_{PID}^2(i) + \chi_{kine}^2$.
- [19] The significance S is calculated by $S = [-2 \times (\ln L_2 - \ln L_1)]^{1/2}$, where L_1 and L_2 is the likelihood function value in the fit with and without signal, respectively.
- [20] J. Conrad *et al.*, Phys. Rev. **D 67**, 012002 (2003). We use the modified likelihood ratio ordering including the systematic uncertainties of signal (Gaussian parametrization) and background (flat parametrization) in confidence interval construction.
- [21] Particle Data Group, S. Eidelman *et al.*, Phys. Lett. **B 592**, 1 (2004).
- [22] BES Collab., J. Z. Bai *et al.*, Phys. Rev. **D 70**, 012005 (2004).
- [23] T. Sjostrand, Comput. Phys. Commun. **82**, 74 (1994).
- [24] J. C. Chen *et al.*, Phys. Rev. **D 62**, 034003 (2000).
- [25] G. Bonneau and F. Martin, Nucl. Phys. **B 27**, 381 (1971).
- [26] CMD-2 Collab., R. R. Akhmetshin *et al.*, Phys. Lett. **B 466**, 392 (1999).
- [27] DM2 Collab., D. Bisello *et al.*, Nucl. Phys. (Proc. Suppl.) **B 21**, 111 (1991).
- [28] CLEO Collab., N. E. Adam *et al.*, hep-ex/0407028.